https://doi.org/10.5194/essd-2023-540
Preprint. Discussion started: 15 January 2024

Open Access Earth System Science Data Discussions

SHIFT: A DEM-Based Spatial Heterogeneity Improved Mapping of Global Geomorphic Floodplains

Kaihao Zheng[1], Peirong Lin[1, 2, *], Ziyun Yin[1]

1. Institute of Remote Sensing and GIS, School of Earth and Space Sciences, Peking University, Beijing, China.
2. International Research Center of Big Data for Sustainable Development Goals, Beijing, China.

* Corresponding author: Peirong Lin (peironglinlin@pku.edu.cn)

Abstract

Floodplain is a vital part of the global riverine system. Among all the global floodplain delineation strategies empowered by remote sensing, DEM-based delineation is considered computationally efficient with relatively low uncertainties, but the parsimonious model struggles with incorporating spatial heterogeneity into the floodplain map. In this study, we propose a globally applicable thresholding scheme for DEM-based floodplain delineation to improve the representation of spatial heterogeneity. Specifically, we develop a stepwise approach to estimate the Floodplain Hydraulic Geometry (FHG) scaling parameters for 269 river basins worldwide to best respect the scaling law while approximating the spatial extent of two publicly available global flood maps derived from hydrodynamic modeling. Based on the spatially-varying FHG parameters, a ~90-m resolution global floodplain map named Spatial Heterogeneity Improved Floodplain by Terrain analysis (SHIFT) is delineated, which takes the hydrologically corrected MERIT-Hydro dataset as the DEM inputs and the Height Above Nearest Drainage (HAND) as the terrain attribute. Our results demonstrate that SHIFT validates well with reference maps with the overall accuracy exceeding 0.85. At the same time, it shows superior consistencies with several other datasets sourced from independent hydrodynamic modeling and DEM-based approaches. SHIFT effectively captures the global patterns of the geomorphic floodplains, with better regional details than existing data. The estimated FHG exponent exhibits a significant positive relation with the basins' climatic aridity conditions, particularly for 34 world's major river basins, suggesting the ability of the scaling exponents in capturing more spatial heterogeneity. SHIFT estimates global

https://doi.org/10.5194/essd-2023-540
Preprint. Discussion started: 15 January 2024


Open Access Earth System Science Data Discussions

floodplain area to be 8.2 million km^2, representing 5.5% of the world's total land area, and we anticipate SHIFT, available at https://zenodo.org/records/10440609 (Zheng et al., 2023), to be used to support a range of applications requiring boundary delineations of the global geomorphic floodplains.

Highlights

- We develop a globally applicable thresholding scheme for DEM-based floodplain mapping that improves the integration of floodplain spatial heterogeneity.
- We create a new 90-m geomorphic floodplain map named Spatial Heterogeneity Improved Floodplain by Terrain analysis (SHIFT).
- SHIFT exhibits better consistency with existing floodplain maps.
- The estimated exponent in Floodplain Hydraulic Geometry (FHG) exhibits significant a positive relation with climatic aridity.
- Global floodplain area is estimated to be 8.2 million km^2, representing 5.5% of the world's total land area.

https://doi.org/10.5194/essd-2023-540
Preprint. Discussion started: 15 January 2024

Open Access Earth System Science Data Discussions

1. Introduction

Floodplain is an integral component of the global riverine system – it acts as a river's ecological buffer, and offers conveniences for human settlements while also harboring flood risks (Di Baldassarre et al., 2013). Floodplains accommodate over half of the world's human habitation and development due to their favorable nature (Andreadis et al., 2022; Best, 2019). Thus, accurate delineation of floodplain boundaries has attracted wide attention among ecologists, flood practitioners/engineers, and geomorphologists (Wohl, 2021). Among various mapping efforts across different scales and resolutions (Dhote et al., 2023), global-scale floodplain maps are particularly valuable as they require a consistent and spatially continuous framework, which can be leveraged to offer insights into the changing global floodplain characteristics and flood risks (Du et al., 2018; Lindersson et al., 2020; Rajib et al., 2021, 2023; Rentschler et al., 2022, 2023).

Terrestrial observation empowered by satellite remote sensing provides essential data that allow for the delineation of global-scale floodplain by estimating inundation caused by flood extremes. One strategy for the delineation is to directly detect the flood inundation areas from optical or Synthetic Aperture Radar (SAR) remote sensing imageries (e.g., Tellman et al., 2021). This requires historical occurrence of a flood event to define a floodplain, but such an event-based approach often results in spatially discrete global floodplain maps limited by satellite data quality and accessibility. It also overlooks unflooded yet at-risk locations, potentially underestimating floodplain extents. Other strategies involve running hydrodynamic or hydraulic models, which takes input data from terrain and runoff forcing and then simulate detailed flood inundation dynamics in a computationally demanding manner (Bates et al., 2018; Trigg et al., 2021). This method derives continuous floodplain maps, and it emphasizes the inundation area under different flood return periods (e.g., 100-year floodplain), which is more commonly used in engineering and hazard mitigation practices (Wohl, 2021). Various global floodplain maps are available from different hydrodynamic models, including the European Commission's Joint Research Centre (JRC) (Dottori et al., 2016), the CIMA-UNEP model from the Global Assessment Report (GAR) (Rudari et al., 2015), CaMa-Flood (Yamazaki, 2014), Fathom Global (Sampson et al., 2015) and GLOFRIS (Winsemius et al., 2013). Yet due to the uncertainties that concern the forcing inputs, model structure and parameters, notable inconsistencies are reported across these datasets (Bates, 2023; Bernhofen et al., 2022; Trigg et al., 2016). Thus, the uncertainties associated with the above

https://doi.org/10.5194/essd-2023-540
Preprint. Discussion started: 15 January 2024

approaches highlight the need for continuous efforts to improve global floodplain mapping strategies.

Recent advancements in remote sensing offer ever-growing spatial coverage, refined resolution and improved accuracy of global terrain products, motivating the third strategy to directly delineate floodplains with satellite-derived terrain data. The Digital Elevation Models (DEMs)-based or terrain analysis approach is often considered to exhibit higher computational efficiencies as it takes less data and parameters, and the sufficiently accurate DEMs are already recognized as the least uncertain component compared to other uncertainty sources in global floodplain mapping with hydrodynamic models (Bates, 2023). As a result, the parsimonious DEM-based floodplain mapping method receives growing attention in large-scale studies and ungauged basins (Manfreda et al., 2014; Nardi et al., 2013, 2018; Tavares da Costa et al., 2019). DEM-based floodplain mapping generally consists of two steps. First, essential terrain attributes such as Height Above Nearest Drainage (i.e., HAND), Topography Wetness Index, Slope Position, or their derivatives are calculated from DEMs to represent river proximity (Beven and Kirkby, 1979; Rennó et al., 2008; Weiss, 2001; Xiong et al., 2022). Second, thresholding schemes are applied to these attributes to delineate the floodplain boundary (Dhote et al., 2023). For example, the GFPlain algorithm, a widely applied method for terrain-based floodplain delineation (Knox et al., 2022; Manfreda et al., 2014; Nardi et al., 2006; Rajib et al., 2023), adopts such an approach to create the GFPlain250m dataset (Nardi et al., 2019). In a recent comparative study, GFPlain250m was proved to show the highest consistency with several existing floodplain maps, highlighting the potential of geomorphic floodplain delineation in reducing model uncertainties (Lindersson et al., 2021).

However, DEM-based mapping methods also face challenges particularly in characterizing spatial heterogeneity (Annis et al., 2019), or spatial variations of floodplain characteristics and processes discovered across scales such as topography, morphology, climate, stratigraphy, biodiversity and river fluxes (Iskin and Wohl, 2023; Wohl, 2021; Wohl and Iskin, 2019). In a DEM-based mapping approach, one needs to address the impact of heterogeneous factors on floodplain extents through thresholding schemes, but currently there is no universal large-scale thresholding scheme available (Dhote et al., 2023). Many previous attempts assume homogeneous determining factors within the study area and directly assume a universal threshold (e.g., a specific HAND threshold for all pixels)

https://doi.org/10.5194/essd-2023-540
Preprint. Discussion started: 15 January 2024


Open Access Earth System Science Data Discussions

in obtaining geomorphic floodplains, which may suffice at smaller scales but could significantly skew results in large-scale studies (Afshari et al., 2018; Hocini et al., 2021; Manfreda et al., 2014; Nardi et al., 2013). To better account for spatial heterogeneity, the aforementioned GFPlain algorithm (Nardi et al., 2006) applied the floodplain hydraulic geometry (hereafter FHG, Bhowmik, 1984) as the thresholding scheme. In the FHG scaling law relationship, the floodplain extent scales exponentially with the river's upstream drainage area (UPA), which adds UPA as the primary determining factor in deriving floodplain maps. However, it often adopts universal values for FHG parameters across basins (Nardi et al., 2019), implying that other sources of heterogeneity encapsulated by the FHG scaling parameters is ignored. While studies attempting to estimate the empirical parameters of FHG with statistical fitting methods exist, it remains difficult to derive FHG parameters worldwide and to offer further physical interpretations for the parameters. Such inadequate representation and understanding of spatial heterogeneity in FHG parameters may lead to inaccurate delineations in less well-documented regions; for example, overestimated floodplains in arid or semi-arid area as reported by existing assessments of geomorphic floodplains (Dhote et al., 2023; Lindersson et al., 2021).

To complement existing studies, here we develop a globally applicable framework to estimate FHG parameters that better integrate spatial heterogeneity into our thresholding scheme. It takes two publicly available hydrodynamic floodplain maps as the reference to estimate spatially varied FHG parameters across 269 global river basins. Based on this, we develop a 90-m global geomorphic floodplain map named Spatial Heterogeneity Improved Floodplain by Terrain analysis (SHIFT). SHIFT calculates HAND above the nearest river pixel to which it drains by utilizing the hydrologically corrected MERIT-Hydro (Yamazaki et al., 2019) dataset. Due to the use of the MERIT-Hydro dataset, SHIFT also addresses limitations of existing global geomorphic mapping that used uncorrected DTM with limited spatial coverages (60°N to 60°S) and relatively low spatial resolutions. Our manuscript is organized as the follows. Section 2 introduces our methods and data in detail. Section 3 presents our geomorphic floodplain data and the accuracy assessment against several reference maps. Sections 4 & 5 close with discussions and conclusions of this study.

https://doi.org/10.5194/essd-2023-540
Preprint. Discussion started: 15 January 2024

Open Access Earth System Science Data Discussions

3. Methods and Data

SHIFT is developed following the technical flowchart in **Fig. 1**. Below we will describe our data and methods in detail.

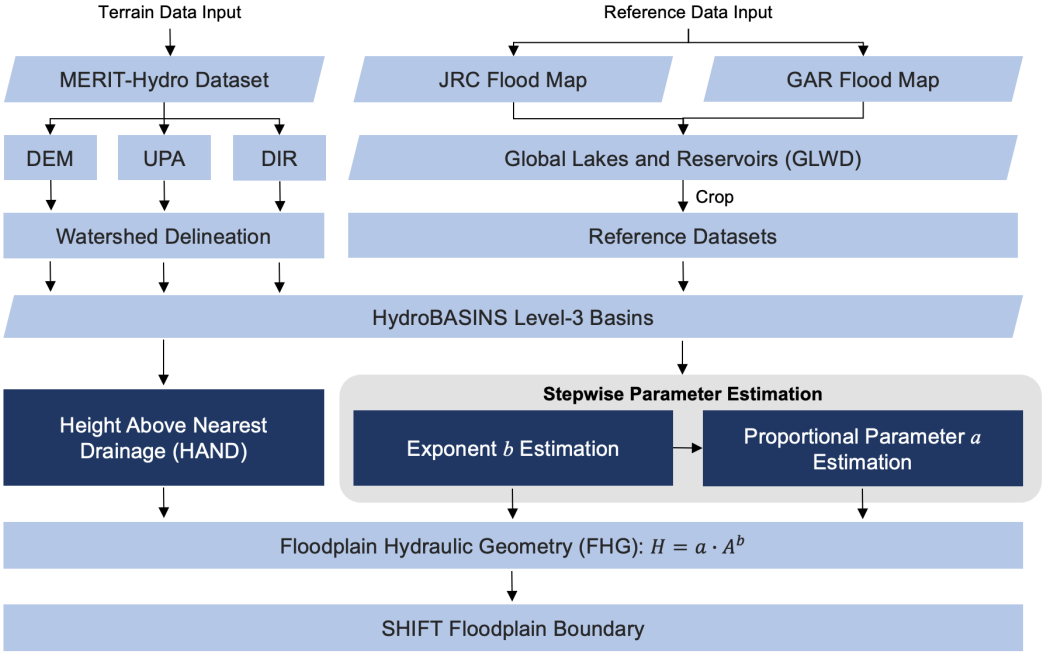

Fig 1. Technical workflow of the study. Parallelograms denote data; rectangles denote processing; highlighted rectangles are the key features of SHIFT. Stepwise parameter estimation is marked in the grey box.

2.1 Data

(1) MERIT-Hydro hydrography map. We take terrain inputs (i.e., elevation, d-8 flow direction and upstream drainage area) from the MERIT-Hydro dataset (Yamazaki et al., 2019). It is a 90-m resolution global dataset that combines data from the Space Shuttle Radar Topography Mission (SRTM) and airborne LiDAR, which has undergone rigorous error correction processes to remove various types of errors such as striping noise, speckle noise, absolute errors, as well as biases in tree heights. Multiple remote sensing datasets and Volunteer Geographic Information System

https://doi.org/10.5194/essd-2023-540
Preprint. Discussion started: 15 January 2024

(Volunteer GIS) water data are used to further enhance its ability to identify river locations. Specifically, it combines OpenStreetMap river vector data, SRTM waterbody data, and Landsat-derived water data to calculate the likelihood of a grid cell representing a water body. In areas with a high likelihood of water, the elevation is adjusted lower. This approach effectively improves the accuracy of flow direction calculations and minimizes deviations in flat areas. The dataset is georeferenced to the WGS84 and EGM96 geodetic reference systems, with a spatial resolution of 3 arc-seconds (approximately 90 meters at the equator).

(2) HydroBASINS Level-3 Global Basins. We applied basin boundary data from the level-3 HydroBASINS dataset to introduce the basin-by-basin spatial variability in parameter estimation. It is a multi-level global basin dataset derived from the SRTM DEM data as part of the HydroSHEDS project (Lehner and Grill, 2013). HydroBASINS is structured into 12 levels of basins, with higher levels representing finer basins. The dataset applies the Pfafstetter coding system to support analysis of watershed topology including upstream and downstream connectivity. The first three levels are assigned with Level 1 categorizing continents, Level 2 dividing continents into major sub-units, and Level 3 delineating the largest river basins on each continent (Lehner, 2014). The Level-3 sub-basins in HydroBASINS consist of 269 units globally with an average size of 555,600 km^2. Among them, 34 major river basins with complete coverage between 60°N to 60°S (the spatial extent of our reference maps, see below) are used for further analysis in Section 4.1.

(3) JRC flood map. The flood hazard map created by the European Commission's JRC is selected as part of the reference and validation dataset. It is based on the 3-arcsecond SRTM DEM, which combines hydrological simulations from the Global Flood Awareness System (GloFAS) with a two-dimensional CA2D hydraulic model for flood inundation mapping. The GloFAS simulations utilize ERA-Interim data, covering the period from 1980 to 2013, and operate at a resolution of 0.1 degrees (approximately 11 km at the Equator). The system simulates streamflow by coupling two distributed global models: HTESSEL, which estimates surface water and energy fluxes in response to atmospheric forcing, and LISFLOOD Global, which uses the output from HTESSEL to simulate routing processes and streamflow. The flood hazard maps produced are at a 30-second resolution and focus on river channels with an upstream catchment area greater than 5000 km^2

https://doi.org/10.5194/essd-2023-540
Preprint. Discussion started: 15 January 2024

(Dottori et al., 2016). The JRC dataset provides flood hazard maps with different return periods from 10 years to 1000 years. Here we used the 500-year flood map as a reference floodplain map based on the notion that geomorphic floodplains are dominantly shaped by high-impact yet low-possibility events (Annis et al., 2019; Bhowmik, 1984; Lindersson et al., 2021).

(4) GAR flood map. We also select the 500-year flood map by hydrodynamic model from the GAR of the United Nations Office for Disaster Risk Reduction (UNDRR) and the CIMA foundation as a reference and validation dataset. The GAR data employs a global database of discharge data from over 8000 stations to estimate extreme streamflows and DEM from HydroSHEDS for hydraulic modeling. This one-dimentional model applies Manning's equation to calculate river stages. The GAR flood map also considers artificial flood defense by assuming target return periods of flood defenses based on the GDP distribution, thereby locally reducing the estimated flooded volume within the estimated protected area. The dataset is characterized by return periods of 25, 50, 100, 200, 500, and 1000 years, a coverage of 60°N to 60°S, with a native resolution of 90 meters from the SRTM DEM, later aggregated to 1 km for risk computation (Rudari et al., 2015).

(5) GFPlain250m floodplain map. The aforementioned geomorphically delineated GFPlain250m floodplain map is used as the benchmark and another validation dataset (Nardi et al., 2019). It shares the same coverage with GAR (60°N to 60°S). For each grid, it calculates the height above the lowest elevation grid within the same watershed (i.e., the basin outlet) as the terrain attribute rather than the nearest river grid to which it drains. This may lead to underestimation of floodplain in upstream areas. FHG is applied as the thresholding scheme (Nardi et al., 2006), but the exponent takes universal values across different basins (i.e., exponential parameter b = 0.3, proportional parameter a = 0.01) for convenient global applications. It takes the 250 m SRTM DTM as terrain input and implements the hydrological analysis workflow by using the ArcPy library.

(6) GLWD lake and reservoir dataset. We apply a global lake mask to crop the reference map before using it for parameter estimation, which helps to avoid inconsistent lake representations from our reference and validation datasets. To do that, the Global Lake and Wetland Dataset (GLWD) jointly developed by the World Wildlife Fund (WWF) and the Center for Environmental Systems Research at the University of Kassel (Lehner and Döll, 2004) is used. It consists of three

https://doi.org/10.5194/essd-2023-540
Preprint. Discussion started: 15 January 2024

layers and the Level-1 layer represents large lakes and reservoirs, including 3,067 lakes and 654 reservoirs with lake area ≥ 50 km² and storage capacity ≥ 0.5 km³, respectively. The dataset takes reference from multiple sources and is further refined with independent data from USGS and extensive visual inspections and quality control.

(7) Global-AI_PET_v3 Aridity Index database. We use the Aridity Index (AI) from the Global Aridity Index and Potential Evapotranspiration Database (Global-AI_PET_v3) to assess its linkage with the FHG parameter. The database provides 30 arc-second global Potential Evapotranspiration (ET_0) and AI data. AI is calculated as the ratio of mean annual precipitation to mean annual reference ET_0, which is estimated by the FAO Penman-Monteith Reference Evapotranspiration equation. It has been validated against various weather station data and shows an improved correlation with real-world data compared to previous versions (Zomer et al., 2022).

2.2 Methods

This section introduces HAND, FHG and our parameter estimation scheme for SHIFT.

(1) HAND as a terrain attribute. HAND is a derivative terrain index that describes the relative elevation difference between any grid cell in a DEM and its nearest river grid (Rennó et al., 2008). River grid here is identified by applying a 1000 km^2 threshold to the Upstream Drainage Area (UPA). Accurate HAND calculation requires defining the nearest river network grids either by flow direction or by distance. The flow direction model defines the first river network grid reached by tracing the d-8 flow as the nearest drainage, resulting in floodplain maps that capture regional hydrological characteristics but influenced by local terrain fluctuations. The distance model searches for the nearest drainage grid with a specific distance (e.g., two-dimensional or three-dimensional Euclidean distance), highlighting geometric considerations but ignores natural geomorphic separations. We adopt the flow direction method to avoid discontinuities in HAND introduced by the distance model (not shown); subsequent results in floodplain delineation are derived from using the d-8 flow directions obtained from the MERIT-Hydro dataset.

(2) FHG as a thresholding scheme. FHG is an adapted form of the original river channel hydraulic geometry (Leopold and Maddock, 1953). It posits a power-law relationship between floodplain

https://doi.org/10.5194/essd-2023-540
Preprint. Discussion started: 15 January 2024

characteristics (width, depth, 100-year discharge) and river size (UPA or strahler stream order). In the context of floodplain delineation, it considers a power-law relationship between the potential inundation depth (h) of a river grid cell and its UPA:

$$h = a \cdot UPA^{b} \quad (1)$$

where a and b are empirical parameters containing heterogeneous factors determining floodplain extents. Then, the algorithm determines grid cells with HAND lower than h of the corresponding river grid (h_{river}) as floodplain, which can be represented by Eq. (2):

$$f(HAND, h_{river}) = \begin{cases} 1, HAND \leq h_{river} \\ 0, HAND > h_{river} \end{cases} \quad (2)$$

(3) FHG parameter estimation. Estimating FHG parameters requires either reference floodplain extents or estimated runoff as inputs (Annis et al., 2019; Nardi et al., 2013). We take two hydrodynamic model outputs as the reference map (i.e., the 500-year return period JRC and GAR flood maps) as they intrinsically contain floodplain spatial heterogeneity by feeding gauged streamflow observations or climate reanalysis data (Lindersson et al., 2021). For areas where both maps are available, we take both the join and the interserction of JRC and GAR as the reference, as we consider the intersection map to be accurate and the union map to be comprehensive. For areas above 60°N, we take the JRC as the reference since it is the only map available.

With the above reference map, two methods can be used to estimate FHG parameters: parameter space sampling (PSS) and logarithmic regression (LR). PSS defines a feasible range for two parameters in Eq. (1), and then samples the parameters from the parameter space and tests their combinations against a reference map by using a fitness index (Annis et al., 2019). LR assumes that all floodplain grids from the reference map satisfy the scaling law so that the FHG parameters b and a can be estimated by statistical approximation (Nardi et al., 2013). For LR, we expect all floodplain pixels in the reference map to satisfy:

$$HAND \leq a \cdot UPA_{river}^{b} \quad (3)$$

https://doi.org/10.5194/essd-2023-540
Preprint. Discussion started: 15 January 2024

which could be transformed into:

$$ln(HAND) \leq b \cdot ln\,(UPA_{river}) + ln\,(a) \quad (4)$$

Apparently, PSS can best approximate the output but could lead to equifinality, while LR emphasizes the scaling law but could be influenced by uncertainties of the reference data (see more details below). Therefore, we combine the two methods above and propose a stepwise parameter estimation framework. Specifically, we first determine baseline values for parameter a_0 from prior research, then estimate b by forcing logarithmic regression based on the reference dataset to best respect the FHG scaling law; then, the coefficient a is calculated by sampling parameter space based on the reference map and the determined b value.

Equation (4) anticipates a positive linear relationship (**Fig. 2a**) between ln(UPA_{river}) and the maximum ln(HAND) values that mark the furthest floodable grid by each river grid, but our observations deviate from this expectation because some river grids with small drainage areas can have unexpectedly high HAND values. These can be ascribed to uncertainties with our reference map that inherits the model chain errors, terrain data and spatial resolution inconsistencies, as well as other unaccounted within-basin variability that may break the scaling law. While results from the Gaussian kernel density plot (**Fig. 2b**) prove that the majority of data still conforms to the power law, the patterns indicates that one cannot simply apply LR to the maximum ln(HAND) and ln(UPA_{river}) to obtain the required parameters.

https://doi.org/10.5194/essd-2023-540
Preprint. Discussion started: 15 January 2024

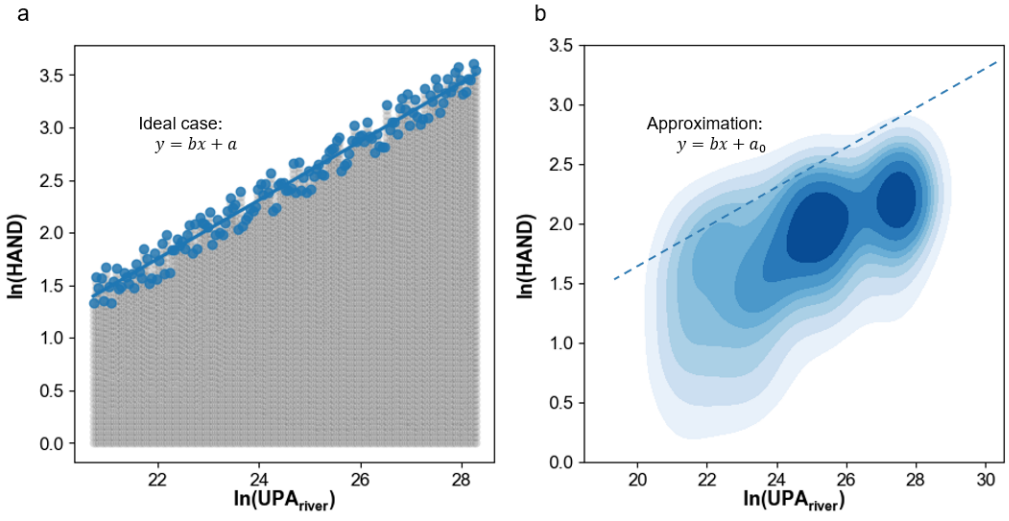

Fig 2. The expected and actual scenario of floodplain grids within a basin. X-axis represents ln(UPA$_{river}$), y-axis represents ln(HAND). a) shows the scatter plot of the expected linear relationship between maximum ln(HAND) and ln(UPA$_{river}$). Blue scatters are the maximum HAND values while gray scatters are non-maximum reference floodplain grids. b) shows the actual scenario (i.e., the Yangtze River basin, BasinID: 4002082) which approximately arrives at the power law relationship in kernel density plot.

Therefore, we develop a scheme to effectively mitigate data noises in estimating parameter *b* while maintaining the power law for the majority of grids. First, we take floodplain grids from the less noisy intersection reference map and set a universal HAND threshold of 20 m to screen out the most obvious high anomalies. We then group HAND values by UPA$_{river}$ and apply an iterative moving-window data-filtering scheme based on 3-sigma statistics where every grid would be filtered by 20 windows (window size = 1, step = 0.1). In each iteration, we compute the mean and standard deviation for the data within each window. A grid point is retained only if it consistently meets the 3-sigma criteria across all 20 windows. This iterative process stops either when every data point fits within all moving windows, or if the procedure fails to converge towards a stable solution. Instead of directly performing LR, we calculate a sequence of theoretical *b* values from the maximum HAND of each UPA$_{river}$ unit with a baseline estimate of a_0= 0.01 based on prior research (Nardi et al., 2019). As the optimal *b* will lean towards the higher end of our calculated

https://doi.org/10.5194/essd-2023-540
Preprint. Discussion started: 15 January 2024

sequence but not at the highest end as it could be possibly interfered by remaining high HAND anomalies, we evaluate the 10% to 50% percentiles of these b sequences across all basins to identify the best percentile that centers around the previously estimated global b value of 0.3 (Nardi et al., 2019). The b value under this identified percentile is then chosen as the optimal parameter for each individual basin.

After b is determined, the coefficient a is optimized with an iterative PSS method. We take both the intersection map and the union map as our reference dataset, as we would like to highlight the 'consensus' of existing maps while trying to capture more spatial heterogeneity from both maps. We apply the Overall Accuracy (OA) as the target in the parameter estimation process:

$$OA = \frac{A + D}{A + B + C + D} \tag{5}$$

A, B, C, D denote overlapping (True Positive), over-predicition (False Positive), under-prediction (False Negative), and correct rejection (True Negative), respectively. We select OA instead of kappa coefficient (Cohen, 1960), Model Agreement Index (Trigg et al., 2016) or measure-of-fit function (Nardi et al., 2019), because other indices can be less appropriate in our case as we use a composite of two largely inconsistent hydrodynamic flood maps. Approximation by these indices would focus on predicted areas by either dataset and may overlook non-floodplain areas, which could lead to overestimation in parameters and thus floodplain extents. Considering the previously estimated a values range across 0.001 to 0.06 (Nardi et al., 2018), we first sample 20 equidistant a values between 0 and 1 against the reference data. Then the direct neighbor of the best-performing a value, constraining its precision to at least one decimal place, is used to search for the true optimal a. We apply four iterations, each with a new set of 20 equidistant a values within the estimated direct neighbors from the last iteration. The optimal a from the final iteration is then selected as the as the basin-specific coefficient.

(4) Development of SHIFT. Based on the above, we estimate the FHG parameter with the HydroBASINS level-3 basins, and derive the floodplain map for each basin and then integrate them into a 90 m global floodplain map. We use Python 3.10 libraries (e.g., Pandas, Numpy and

https://doi.org/10.5194/essd-2023-540
Preprint. Discussion started: 15 January 2024


Open Access Earth System Science Data Discussions

Geopandas), the GDAL command line interface and the TauDEM toolkit (Terrain Analysis Using Digital Elevation Models (TAUDEM)) for the FHG parameter estimation and the thresholding. We also downsize the dataset to 1-km resolution floodplain map for convenient large-scale applications, and the 1-km resolution floodplain map is provided as part of the final output. Permanent water bodies are removed for all processes.

(5) Validation. Finally, we conduct a pairwise consistency analysis among four floodplain maps, i.e., SHIFT, GFPlain250m, JRC and GAR to ensure the quality of SHIFT. We also apply OA and Model Agreement Index (MAI, see Eq. 6) for this pairwise consistency analysis in reference to previous research (Lindersson et al., 2021), where A, B, C in Eq. (6) are the same as Eq. (5).

$$MAI = \frac{A}{A + B + C} \tag{6}$$

A, B, C denote the same as Eq. 5. b has different influence on rivers depending on their drainage area, i.e., large b values highlighting the dominance of large rivers over tributaries in shaping floodplain extents, we expect b to be better associated with the spatial heterogeneity of floodplain characteristics. Therefore, we also calculate the correlation of the exponent b and climate aridity of all basins, which helps to validate whether our thresholding scheme can better capture spatial heterogeneity of global floodplains.

4. Results

3.1 Global FHG parameter estimation

Based on the stepwise parameter estimation scheme proposed in Section 2.2 (3), we obtain the statistical distributions of different b percentiles in **Fig. 3a**. While distributions from all percentiles exhibit similar patterns, especially for the 20th to 50th percentiles, we apply the 30th percentile worldwide as it best distributes around the previously estimated global b value of 0.3 (Nardi et al., 2019; see dashed line in **Fig. 3a**). Under this percentile, the estimated b values fall within the range of 0.2 to 0.4 across all 269 basins globally, and they exhibit a statistically significant but weak positive correlation (r = 0.281) with the climatic aridity of all basins. Notably, it exhibits a reasonably strong correlation for 34 global major river basins (r = 0.612, **Fig. 3b**).

https://doi.org/10.5194/essd-2023-540
Preprint. Discussion started: 15 January 2024

Spatially, the distribution of the estimated *b* (**Fig. 3c**) shows that regions characterized by abundant precipitation and water resources (e.g., southern East Asia, Southeast Asia, the Mississippi and Amazon) generally exhibit relatively higher *b* values. Conversely, regions such as Central-West Asia, the Arabian Peninsula, the Sahara region, and central Australia tend to have relatively lower *b* values. There are also exceptions, for instance the overall high b values in the arctic circle, low values in river deltas (e.g., Red river in North America, Jiaodong Penninsula in Eastern Asia) along with the high anomalies in the Great Victoria Desert in Australia. Based on the estimated *b*, the coefficient *a* is also optimized which varies from 0.0001 to a maximum of 0.2 across all basins.

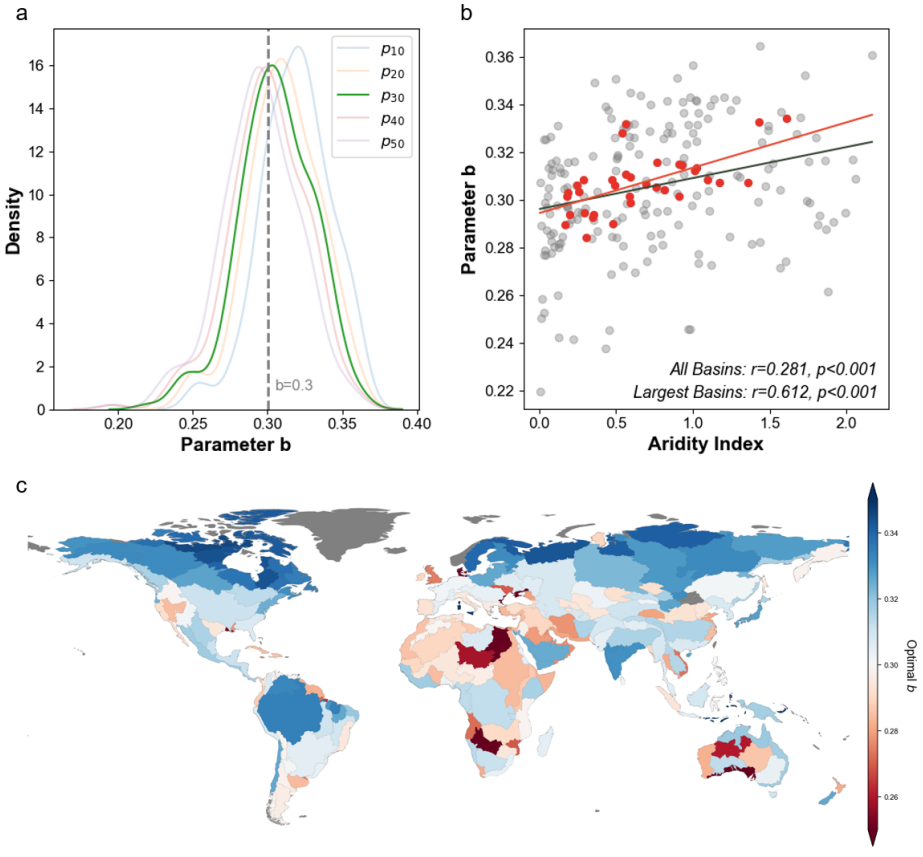

Fig 3. Results of FHG parameter b estimation. a) The distribution of parameter *b* across basins, p_{10} to p_{50} represent the percentiles during estimatio, $b = 0.3$ line shows the universal value applied in previous research. b) Scatter plot with regression line for Aridity Index and parameter *b*, gray

https://doi.org/10.5194/essd-2023-540
Preprint. Discussion started: 15 January 2024

scatters stand for all basins and red scatters for major basins. c) Spatial distribution of parameter *b* across HydroBASINS level-3 basins.

3.2 Global floodplain delineation

Based on the estimated FHG parameters, the global distribution of floodplain areas is delineated and shown in **Fig. 4a**. Overall, the spatial pattern of the floodplains aligns well with the low-lying areas in major river systems. More specifically, floodplains in Northern Asia are mainly distributed around the West Siberian Plain and the Central-West Siberian Plateau, e.g., the Ob and Yenisei River Basins. West and Central Asia's floodplains are primarily near the Caspian Sea, the Aral Sea, and the Mesopotamian Plain. In East Asia, the Yangtze River Basin dominates floodplains in the middle and lower reaches, along with contributions from the North China Plain, some Yellow River tributaries such as the Hetao Plain, and river mouths in the southeast. The Lancang-Mekong River Basin and the Salween-Irrawaddy River Basin in Southeast Asia also breed the largest floodplains worldwide, as well as the Indus and Ganges-Brahmaputra River Basins from South Asia. In Europe, the primary floodplains are concentrated in the Danube River Basin between the Alps and the Carpathian Mountains, alongside the Rhine, Dnieper and Po River Basins. In Africa, floodplains are predominantly distributed in the upstream Nile River, including the Nile Delta and the Niger River Basin, as well as the Congo River Basin, the Chari River-Lake Chad Basin and around Lake Victoria, with additional areas near West and East Africa's coasts. North America's floodplains are mainly in the Mississippi River Basin and Alaska's Yukon River Basin. South America's floodplains are primarily in the Amazon River Basin, the Orinoco plain, and the La Plata plain. In Oceania, floodplains center around the Murray-Darling River Basin in the interior lowlands.

To show more regional details, we use two cases under different climatic conditions (**Figs. 4b & 4c**) to further illustrate the differences between SHIFT and the widely used GFPlain250m dataset. Case 1 (**Fig. 4b**) is the Indus-Ganges-Brahmaputra River basin which flows through Bangladesh, India, Pakistan, and Nepal. These countries are primarily characterized by frequent floods and are strongly influenced by the South Asia monsoon. SHIFT captures detailed floodplains in the Indus River basin, a major basin in South Asia where GFPlain250m leaves out. Additionally, SHIFT offers finer details in upstream areas and can better distinguish main river floodplains from those of the tributaries. Case 2 (**Fig. 4c**) is situated in the Yellow River basin (Hetao Plain) in Inner

https://doi.org/10.5194/essd-2023-540
Preprint. Discussion started: 15 January 2024

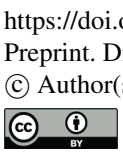

Mongolia, China, a region dominated by arid to semi-arid continental climate. Comparing the floodplain maps with visual interpretations of the satellite images suggests that SHIFT can provide a more comprehensive depiction of the Hetao Plain. The floodplains outside of the Hetao Plain in SHIFT are relatively limited, which aligns with its generally dry climate conditions.

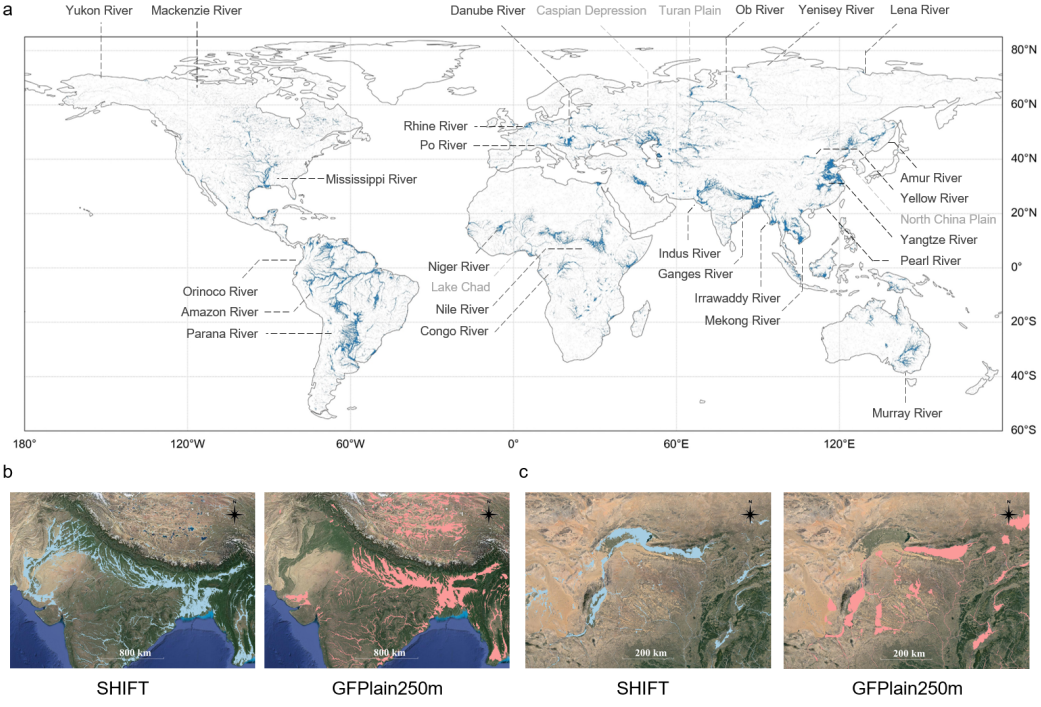

Fig 4. Geomorphic floodplain extent in SHIFT. a) Global spatial distribution of floodplains, with major river basins or plains marked out. b) and c) show two cases of our floodplain delineation and the GFPlain250m dataset, with background image from © Google Earth on EPSG: 3857 projection. b) locates in the humid Indian-Ganges river basin, while c) locates in the semi-arid yellow river basin in inner Mongolia, China.

According to SHIFT, global floodplains take up approximately 8.2 million km^2, representing 5.5% of the world's total land area. **Fig. 5** further shows the floodplain area and percentage of floodplains within each of the global major river basins. Overall, the Amazon River Basin possesses the largest total floodplain area globally (743,294 km^2), followed by the Parana, Nile, Volga and Mississippi River basins. Floodplains in Haihe River Basin takes up the greatest area percentage (~27%),

https://doi.org/10.5194/essd-2023-540
Preprint. Discussion started: 15 January 2024

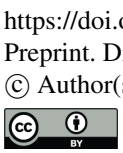

highlighting the great flood inundation potential of such basins. Comparing across continents, South America and Asia breed the most widespread floodplain extent worldwide, while river basins in Asia tend to have the highest floodplain percentages.

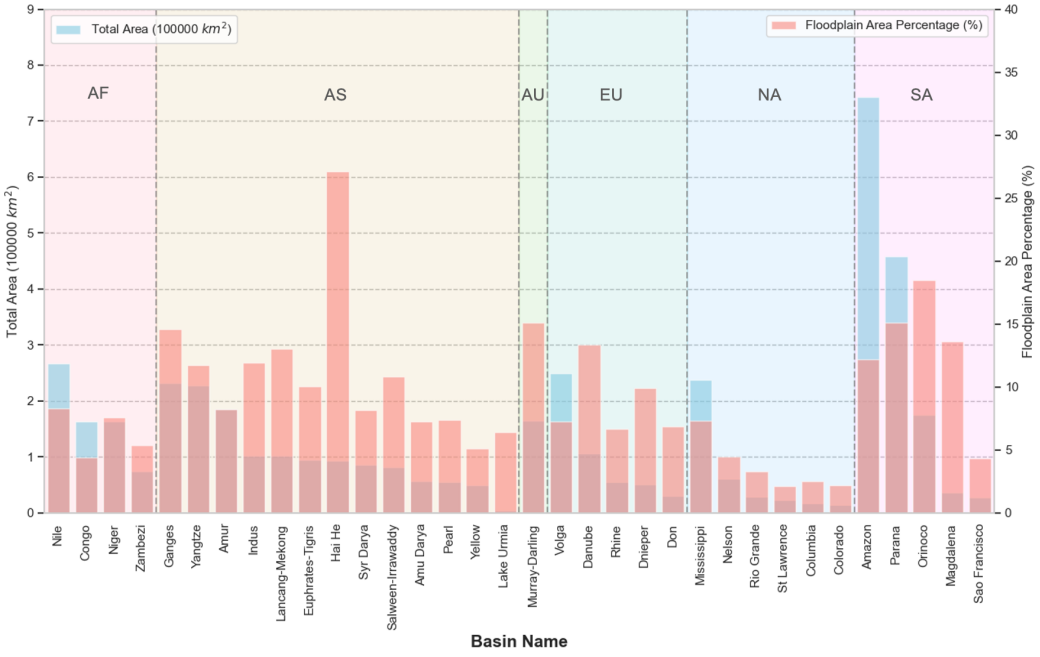

Fig 5. Floodplain area statistics in major river basins. Blue bars stand for total floodplain area (left y-axis), red bars stand for the ratio of floodplain area to the total basin area (right y-axis). Basins are ranked by total floodplain area. AF: Africa, AS: Asia, AU: Australia, EU: Europe, NA: North America, SA: South America.

3.3 Validation and consistency analysis

Figure 6 shows the global basin-level distribution of OA between SHIFT and the reference map that considers both the intersection and union of two hydrodynamic maps (Section 2.1). The results reveal that the algorithm achieves an accuracy of over 0.85 in the majority of global basins, proving the effectiveness of our parameter estimation scheme in capturing information from the reference maps. Regions with well-established floodplain mapping systems (e.g., Danube and Mississippi) tend to show better consistency between reference maps and thus present higher OA, while the

https://doi.org/10.5194/essd-2023-540
Preprint. Discussion started: 15 January 2024

lowest OA are seen in river deltas, including the delta of the Amazon River (OA = 0.56) and the Nile River (OA = 0.73), the Red River in North America (OA = 0.81), as well as the Jiaodong Penninsula in East Asia (OA = 0.81). Most basins perform better against the intersection map compared to the union map due to large inconsistency between the two reference maps themselves. The arctic basins and arid regions (e.g., the Sahara, Mongolia, and central Australia) present highest OA against both reference datasets due to the very limited floodplain distribution there.

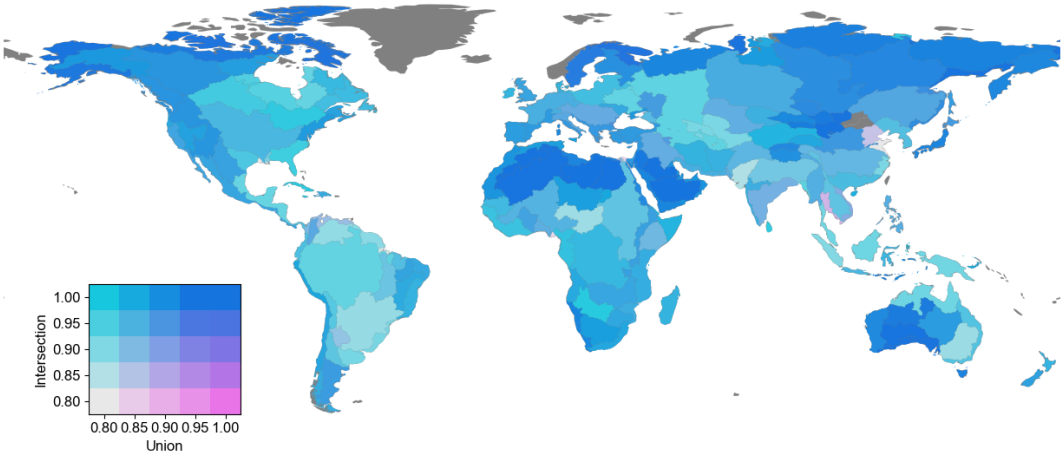

Fig 6. Validation of SHIFT against two reference datasets. Two variables in the bivariate map are the OA against the union map (magenta) and the intersection map (cyan). Balanced OAs will result in blue basins.

Fig. 7a shows the statistics of the pairwise consistency analysis among different floodplain maps (i.e., SHIFT, JRC, GAR, GFPlain250m). Overall, the highest MAI is observed between GAR and GFPlain250m, as well as the SHIFT and JRC pair (blue box, **Fig. 7a**), demonstrating the superiority of geomorphic mapping approaches, and such a pattern is more prominent when considering 34 major basins only (orange box, **Fig. 7a**). For example, the consistency between SHIFT and JRC surpassed that between GAR and GFPlain250m. In the remaining pairs, SHIFT consistently presents higher MAI with other validation datasets. The high MAI between GAR and GFPlain250m is likely the result of overestimation, especially in GAR, as evidenced by the lowest OA values for all pairs involving GAR. In contrast, SHIFT consistently shows the highest OA

https://doi.org/10.5194/essd-2023-540
Preprint. Discussion started: 15 January 2024


Open Access Earth System Science Data Discussions

values with existing pairs, both in GAR pairs and non-GAR pairs. Such patterns of high MAI but low OA concerning GAR reveal the complex dynamics between consistency and accuracy.

To better understand the spatial variation in pairwise analysis, we plot the most consistent pair and corresponding MAI values for each basin (**Fig. 7b**). We find that basins with SHIFT as their highest-consistency pair are typically located in humid to sub-humid basins, including most major basins such as the Mississippi, Amazon, Yangtze, and Nile. In contrast, basins with GAR and GFPlain as the highest-consistency pairs are generally distributed in arctic basins and arid to semi-arid regions (e.g., the Sahara and Central Australia) where both maps delineate floodplains more extensively than expected. These results further prove that SHIFT can effectively capture spatial heterogeneity encapsulated in the reference datasets. At the same time, it also exhibits high consistency with existing datasets, while better distinguishing between regions with different hydroclimatic conditions.

https://doi.org/10.5194/essd-2023-540
Preprint. Discussion started: 15 January 2024

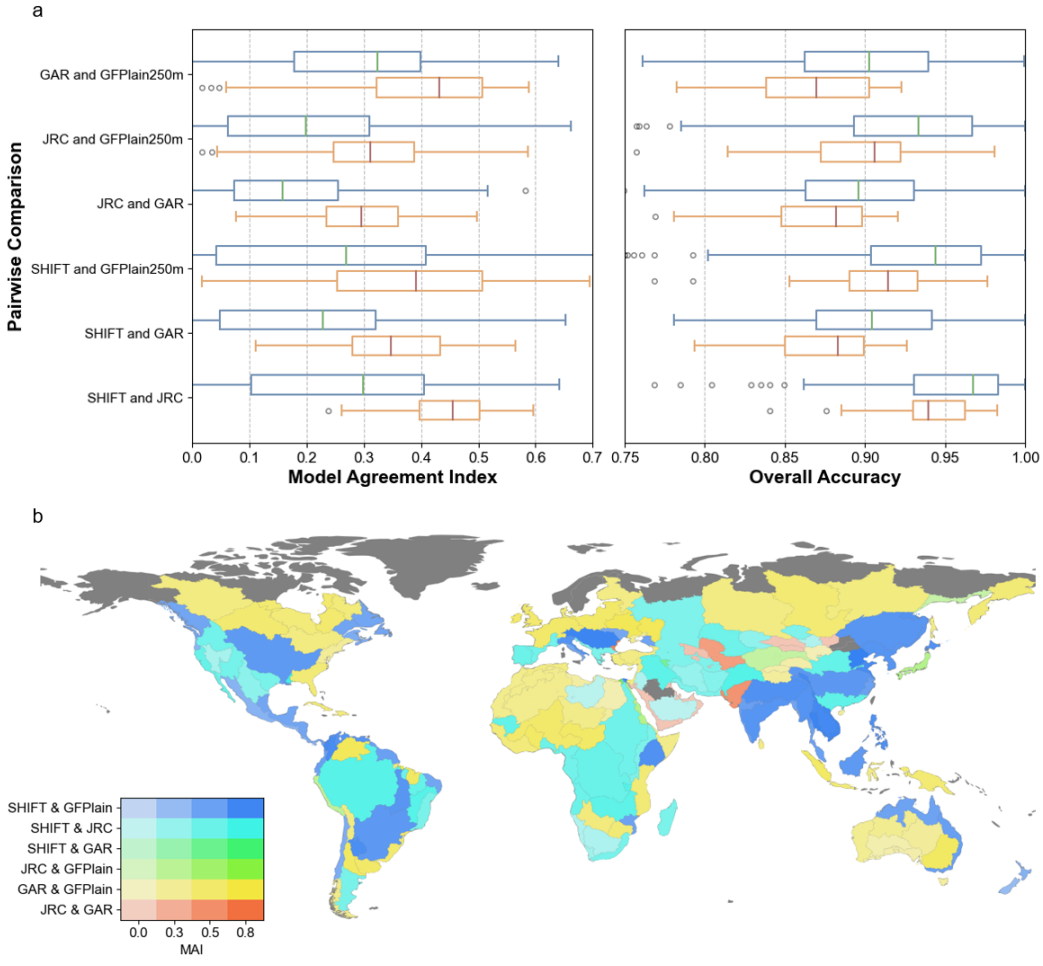

Fig 7. Results of the consistency analysis. a) shows boxplots of pairwise MAI (left) and OA (right) among SHIFT, GFPlain250, JRC and GAR. Statistics for all 269 basins are shown in blue boxes, and that for the 34 major river basins are shown in orange. b) shows bivariate choropleth map of the highest-performance MAI pair and the corresponding MAI value for each basin. Higher MAI results in higher saturation.

4. Discussions

Despite the demonstrated superiority in our approach, several caveats are worth mentioning.

https://doi.org/10.5194/essd-2023-540
Preprint. Discussion started: 15 January 2024

4.1 Uncertainties of the exponent b estimation

During the development of the thresholding scheme, we recognize uncertainties with the FHG relation due to the inconsistencies between the reference maps as well as the data quality across regions. Thus, we quantify the uncertainty of *b* by calculating the standard deviation among all possible *b* values derived at different percentiles, based on the notion that high reference data quality would reduce abnormal HAND values, leading to a narrower range of the estimated *b* sequence and lower standard deviation. While the uncertainty distribution (**Fig. 8**) reveals a complex pattern that does not simply align with the expected *b* patterns shown in **Fig. 3**, areas with limited floodplain (e.g., Western Australia, Central-West Africa, and Central-West Siberia) and mountainous regions (e.g., the Rocky Mountains and the Andes) generally show higher uncertainties (red colors). Recall that we have applied uniform percentiles worldwide to filter data noise, the low uncertainties in regions such as Yangtze, Pearl, Ganges River basins likely suggest a rigorous filter and a subsequently underestimation of *b* may be applied. Yet in the absence of independent data to inform better strategies, we consider our proposed approach valid and effective.

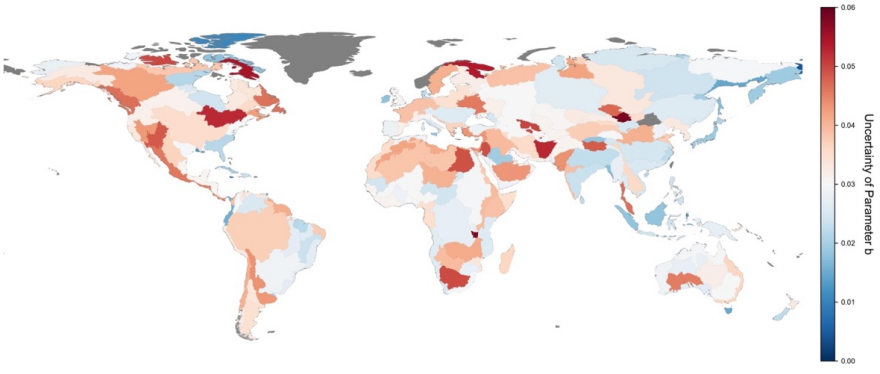

Fig 8. The uncertainty of parameter *b* by basins. Uncertainty is quantified as the standard deviation among all possible b values derived at different percentiles (see Section 2.2 for methods).

4.2 Differentiation between flood inundation and floodplain maps

Geomorphic floodplain maps and inundation maps are fundamentally different, but delineation methods for the latter can be used to delineate the former. Inundation maps have been described as 'hydraulic floodplains' to highlight their engineering uses (Wohl, 2021). In this study, we employ

https://doi.org/10.5194/essd-2023-540
Preprint. Discussion started: 15 January 2024

two 500-year return period flood inundation maps as the reference to estimate floodplain extents, as previous studies imply that geomorphic floodplains are predominantly shaped by low-probability but high-impact flood occurences (Lindersson et al., 2021). It should be noted that our DEM-based approach can be applied to derive FHG parameters based on other return periods, but this study is primarily concerned with exploring the geomorphic characteristics of floodplains rather than focusing on inundation maps on different return periods.

4.3 Spatial scales of SHIFT

The spatially varying parameters for SHIFT are derived based on HydroBASINS Level-3 basins, which depicts 269 river basins in different continents with some containing aggregations of smaller basins. These basins are not hydrologically connected and do not share homogeneous determining factors, thus are suitable for our thresholding scheme that estimates one set of parameters for each basin. A possible strategy to improve the scheme is to further divide these basins into smaller sub-basins, but smaller-scale analysis can increase the impact of reference data uncertainties especially in delta regions with high floodplain discordance (**Fig. 5a**). Considering the high data noise that may limit the further integration of sub-basin level heterogeneity in estimating parameters, the spatial disaggregation scheme used by SHIFT is thought to mark a step forward in improving heterogeneity while offering reasonable physical interpretations of the parameters.

Lastly, when calculating HAND as the terrain attribute for SHIFT, we set an UPA threshold of 1000 km^2 to delineate the river network grids following past studies (Dottori et al., 2016; Nardi et al., 2019; Rudari et al., 2015). A sensitivity test on a smaller threshold (50 km^2) not shown here suggests that more detailed floodplains around smaller rivers can be derived, but at the same time such a threshold can limit expected floodplains by large rivers. Thus, this study considers the 1000 km^2 UPA threshold to be valid. Future large-scale studies can further investigate the above mentioned spatial scale parameters to derive finer maps.

https://doi.org/10.5194/essd-2023-540
Preprint. Discussion started: 15 January 2024

5. Conclusions

In this study, we develop an improved thresholding scheme for large-scale DEM-based floodplain delineation, the core of which being a stepwise estimation framework for Floodplain Hydraulic Geometry (FHG) parameters that respects the power law while better integrating spatial heterogeneity from two publicly available hydrodynamic flood maps. We apply the framework to 269 basins worldwide to derive the required FHG parameters, and the empirical exponent *b* in FHG exhibits reasonable correlations with hydroclimatic conditions, especially for major river basins, proving the effectiveness of our method in better capturing climatic heterogeneity compared to studies that adopt a homogeneous exponent worldwide. Based on the proposed framework, we created a global geomorphic floodplain map named SHIFT (Spatial Heterogeneity Improved Floodplain by Terrain analysis) using terrain inputs from the 90-m MERIT-Hydro dataset, where SHIFT is demonstrated to capture both the global patterns and regional details of geomorphic floodplains well. Global consistency analysis with other floodplain or flood maps from independent data sources further show that SHIFT exhibits superior consistency with existing datasets on a pair-wise basis. We provide the SHIFT data layers at two spatial resolutions (i.e., 90-m and 1-km resolution) for the convenience of the users. Moreover, this research also offers a framework for better understanding FHG parameters and contributes a comprehensive geomorphic floodplain dataset, allowing future large-scale floodplain studies to better capture global patterns and address regional floodplain characteristics.

Author Contribution

Conceptualization: PL. Data curation: KZ, PL, ZY. Formal Analysis: KZ. Funding Acquisition: PL, KZ. Investigation: KZ, PL. Methodology: KZ, PL. Writing – original draft: KZ, PL. Writing – review & editing: KZ, PL, ZY.

Data and Code Availability

SHIFT is openly available at https://zenodo.org/records/10440609 (Zheng et al., 2023). The core codes involved with terrain analysis and FHG parameter estimation is available at https://github.com/Mostaaaaa/SHIFT_floodplain.

https://doi.org/10.5194/essd-2023-540
Preprint. Discussion started: 15 January 2024

Conflict of Interests

The authors declare no conflict of interests.

Acknowledgements

This study is supported by the Open Research Program of International Research Center of Big Data for Sustainable Development Goals, Grant No. CBAS2022ORP05, the National Natural Science Foundation of China (42371481), and Yunnan Science and Technology Major Project (grant NO. 202302AO370012). We acknowledge the funding support from the Fundamental Research Funds for the Central Universities, Peking University on 'Numerical modelling and remote sensing of global river discharge' (no. 7100604136).

Reference

Andreadis, K. M., Wing, O. E. J., Colven, E., Gleason, C. J., Bates, P. D., and Brown, C. M.: Urbanizing the floodplain: global changes of imperviousness in flood-prone areas, Environ. Res. Lett., 17, 104024, https://doi.org/10.1088/1748-9326/ac9197, 2022.

Annis, A., Nardi, F., Morrison, R. R., and Castelli, F.: Investigating hydrogeomorphic floodplain mapping performance with varying DTM resolution and stream, Hydrol. Sci. J., 64, 515–538, 2019.

Bates: Fundamental limits to flood inundation modelling, Nat. Water, 1, 566–567, https://doi.org/10.1038/s44221-023-00106-4, 2023.

Bates, P. D., Neal, J., Sampson, C., Smith, A., and Trigg, M.: Chapter 9 - Progress Toward Hyperresolution Models of Global Flood Hazard, in: Risk Modeling for Hazards and Disasters, edited by: Michel, G., Elsevier, 211–232, https://doi.org/10.1016/B978-0-12-804071-3.00009-4, 2018.

Bernhofen, M. V., Cooper, S., Trigg, M., Mdee, A., Carr, A., Bhave, A., Solano-Correa, Y. T., Pencue-Fierro, E. L., Teferi, E., Haile, A. T., Yusop, Z., Alias, N. E., Sa'adi, Z., Bin Ramzan, M. A., Dhanya, C. T., and Shukla, P.: The Role of Global Data Sets for Riverine Flood Risk Management at National Scales, Water Resour. Res., 58, e2021WR031555,

https://doi.org/10.5194/essd-2023-540
Preprint. Discussion started: 15 January 2024

https://doi.org/10.1029/2021WR031555, 2022.

Best, J.: Anthropogenic stresses on the world's big rivers, Nat. Geosci., 12, 7–21, https://doi.org/10.1038/s41561-018-0262-x, 2019.

Beven, K. J. and Kirkby, M. J.: A physically based, variable contributing area model of basin hydrology / Un modèle à base physique de zone d'appel variable de l'hydrologie du bassin versant, Hydrol. Sci. Bull., 24, 43–69, https://doi.org/10.1080/02626667909491834, 1979.

Bhowmik, N. G.: Hydraulic geometry of floodplains, J. Hydrol., 68, 369–401, https://doi.org/10.1016/0022-1694(84)90221-X, 1984.

Cohen, J.: A Coefficient of Agreement for Nominal Scales, Educ. Psychol. Meas., 20, 37–46, https://doi.org/10.1177/001316446002000104, 1960.

Dhote, P. R., Joshi, Y., Rajib, A., Thakur, P. K., Nikam, B. R., and Aggarwal, S. P.: Evaluating topography-based approaches for fast floodplain mapping in data-scarce complex-terrain regions: Findings from a Himalayan basin, J. Hydrol., 620, 129309, https://doi.org/10.1016/j.jhydrol.2023.129309, 2023.

Di Baldassarre, G., Kooy, M., Kemerink, J. S., and Brandimarte, L.: Towards understanding the dynamic behaviour of floodplains as human-water systems, Hydrol. Earth Syst. Sci., 17, 3235–3244, https://doi.org/10.5194/hess-17-3235-2013, 2013.

Dottori, F., Salamon, P., Bianchi, A., Alfieri, L., Hirpa, F. A., and Feyen, L.: Development and evaluation of a framework for global flood hazard mapping, Adv. Water Resour., 94, 87–102, https://doi.org/10.1016/j.advwatres.2016.05.002, 2016.

Du, S., He, C., Huang, Q., and Shi, P.: How did the urban land in floodplains distribute and expand in China from 1992–2015?, Environ. Res. Lett., 13, 034018, https://doi.org/10.1088/1748-9326/aaac07, 2018.

Hocini, N., Payrastre, O., Bourgin, F., Gaume, E., Davy, P., Lague, D., Poinsignon, L., and Pons, F.: Performance of automated methods for flash flood inundation mapping: a comparison of a digital terrain model (DTM) filling and two hydrodynamic methods, Hydrol. Earth Syst. Sci., 25, 2979–2995, https://doi.org/10.5194/hess-25-2979-2021, 2021.

Iskin, E. P. and Wohl, E.: Beyond the Case Study: Characterizing Natural Floodplain Heterogeneity in the United States, Water Resour. Res., 59, e2023WR035162, https://doi.org/10.1029/2023WR035162, 2023.

Knox, R. L., Morrison, R. R., and Wohl, E. E.: Identification of Artificial Levees in the Contiguous United States, Water Resour. Res., https://doi.org/10.1029/2021WR031308, 2022.

https://doi.org/10.5194/essd-2023-540
Preprint. Discussion started: 15 January 2024

Lehner, B.: HydroBASINS, Global watershed boundaries and sub-basin delineations derived from HydroSHEDS data at 15 second resolution, Technical Documentation Version 1.c, 2014.

Lehner, B. and Döll, P.: Development and validation of a global database of lakes, reservoirs and wetlands, J. Hydrol., 296, 1–22, https://doi.org/10.1016/j.jhydrol.2004.03.028, 2004.

Lehner, B. and Grill, G.: Global river hydrography and network routing: baseline data and new approaches to study the world's large river systems, Hydrol. Process., 27, 2171–2186, https://doi.org/10.1002/hyp.9740, 2013.

Leopold, L. B. and Maddock, T.: The Hydraulic Geometry of Stream Channels and Some Physiographic Implications, U.S. Government Printing Office, 68 pp., 1953.

Lindersson, S., Brandimarte, L., Mård, J., and Di Baldassarre, G.: A review of freely accessible global datasets for the study of floods, droughts and their interactions with human societies, WIREs Water, 7, e1424, https://doi.org/10.1002/wat2.1424, 2020.

Lindersson, S., Brandimarte, L., Mård, J., and Di Baldassarre, G.: Global riverine flood risk – how do hydrogeomorphic floodplain maps compare to flood hazard maps?, Nat. Hazards Earth Syst. Sci., 21, 2921–2948, https://doi.org/10.5194/nhess-21-2921-2021, 2021.

Manfreda, S., Nardi, F., Samela, C., Grimaldi, S., Taramasso, A. C., Roth, G., and Sole, A.: Investigation on the use of geomorphic approaches for the delineation of flood prone areas, J. Hydrol., 517, 863–876, https://doi.org/10.1016/j.jhydrol.2014.06.009, 2014.

Nardi, F., Vivoni, E. R., and Grimaldi, S.: Investigating a floodplain scaling relation using a hydrogeomorphic delineation method: HYDROGEOMORPHIC FLOODPLAIN DELINEATION METHOD, Water Resour. Res., 42, https://doi.org/10.1029/2005WR004155, 2006.

Nardi, F., Biscarini, C., Di Francesco, S., Manciola, P., and Ubertini, L.: Comparing a Large-Scale Dem-Based Floodplain Delineation Algorithm with Standard Flood Maps: The Tiber River Basin Case Study, Irrig. Drain., 62, 11–19, https://doi.org/10.1002/ird.1818, 2013.

Nardi, F., Morrison, R. R., Annis, A., and Grantham, T. E.: Hydrologic scaling for hydrogeomorphic floodplain mapping: Insights into human-induced floodplain disconnectivity: hydrologic scaling and geomorphic floodplain mapping in urban sbasins, River Res. Appl., 34, 675–685, https://doi.org/10.1002/rra.3296, 2018.

Nardi, F., Annis, A., Di Baldassarre, G., Vivoni, E. R., and Grimaldi, S.: GFPLAIN250m, a global high-resolution dataset of Earth's floodplains, Sci. Data, 6, 180309, https://doi.org/10.1038/sdata.2018.309, 2019.

https://doi.org/10.5194/essd-2023-540
Preprint. Discussion started: 15 January 2024

Rajib, A., Zheng, Q., Golden, H. E., Wu, Q., Lane, C. R., Christensen, J. R., Morrison, R. R., Annis, A., and Nardi, F.: The changing face of floodplains in the Mississippi River Basin detected by a 60-year land use change dataset, Sci. Data, 8, 271, https://doi.org/10.1038/s41597-021-01048-w, 2021.

Rajib, A., Zheng, Q., Lane, C. R., Golden, H. E., Jay R. Christensen, Isibor, I. I., and Johnson, K.: Human alterations of the global floodplains 1992–2019, Sci. Data, 10, 499, https://doi.org/10.1038/s41597-023-02382-x, 2023.

Rennó, C. D., Nobre, A. D., Cuartas, L. A., Soares, J. V., Hodnett, M. G., Tomasella, J., and Waterloo, M. J.: HAND, a new terrain descriptor using SRTM-DEM: Mapping terra-firme rainforest environments in Amazonia, Remote Sens. Environ., 112, 3469–3481, https://doi.org/10.1016/j.rse.2008.03.018, 2008.

Rentschler, J., Salhab, M., and Jafino, B. A.: Flood exposure and poverty in 188 countries, Nat. Commun., 13, 3527, https://doi.org/10.1038/s41467-022-30727-4, 2022.

Rentschler, J., Avner, P., Marconcini, M., Su, R., Strano, E., Vousdoukas, M., and Hallegatte, S.: Global evidence of rapid urban growth in flood zones since 1985, Nature, 622, 87–92, https://doi.org/10.1038/s41586-023-06468-9, 2023.

Rudari, R., Silvestro, F., Campo, L., Rebora, N., Boni, G., CIMA Research Foundation, and Christian, C.: Improvement of The Global Flood Model For The [GAR] 2015, UNISDR, 2015.

Sampson, C. C., Smith, A. M., Bates, P. D., Neal, J. C., Alfieri, L., and Freer, J. E.: A high-resolution global flood hazard model, Water Resour. Res., 51, 7358–7381, https://doi.org/10.1002/2015WR016954, 2015.

Terrain Analysis Using Digital Elevation Models (TAUDEM): https://hydrology.usu.edu/taudem/taudem5/.

Tavares da Costa, R., Manfreda, S., Luzzi, V., Samela, C., Mazzoli, P., Castellarin, A., and Bagli, S.: A web application for hydrogeomorphic flood hazard mapping, Environ. Model. Softw., 118, 172–186, https://doi.org/10.1016/j.envsoft.2019.04.010, 2019.

Tellman, B., Sullivan, J. A., Kuhn, C., Kettner, A. J., Doyle, C. S., Brakenridge, G. R., Erickson, T. A., and Slayback, D. A.: Satellite imaging reveals increased proportion of population exposed to floods, Nature, 596, 80–86, https://doi.org/10.1038/s41586-021-03695-w, 2021.

Trigg, M. A., Birch, C. E., Neal, J. C., Bates, P. D., Smith, A., Sampson, C. C., Yamazaki, D., Hirabayashi, Y., Pappenberger, F., Dutra, E., Ward, P. J., Winsemius, H. C., Salamon, P., Dottori, F., Rudari, R., Kappes, M. S., Simpson, A. L., Hadzilacos, G., and Fewtrell, T. J.:

https://doi.org/10.5194/essd-2023-540
Preprint. Discussion started: 15 January 2024

The credibility challenge for global fluvial flood risk analysis, Environ. Res. Lett., 11, 094014, https://doi.org/10.1088/1748-9326/11/9/094014, 2016.

Trigg, M. A., Bernhofen, M., Marechal, D., Alfieri, L., Dottori, F., Hoch, J., Horritt, M., Sampson, C., Smith, A., Yamazaki, D., and Li, H.: Global Flood Models, in: Global Drought and Flood, American Geophysical Union (AGU), 181–200, https://doi.org/10.1002/9781119427339.ch10, 2021.

Weiss, A. D.: Topographic Position and Landforms Analysis, ESRI User Conference, San Diego, 2001.

Winsemius, H. C., Van Beek, L. P. H., Jongman, B., Ward, P. J., and Bouwman, A.: A framework for global river flood risk assessments, Hydrol. Earth Syst. Sci., 17, 1871–1892, https://doi.org/10.5194/hess-17-1871-2013, 2013.

Wohl, E.: An Integrative Conceptualization of Floodplain Storage, Rev. Geophys., 59, https://doi.org/10.1029/2020RG000724, 2021.

Wohl, E. and Iskin, E.: Patterns of Floodplain Spatial Heterogeneity in the Southern Rockies, USA, Geophys. Res. Lett., 46, 5864–5870, https://doi.org/10.1029/2019GL083140, 2019.

Xiong, L., Li, S., Tang, G., and Strobl, J.: Geomorphometry and terrain analysis: data, methods, platforms and applications, Earth-Sci. Rev., 233, 104191, https://doi.org/10.1016/j.earscirev.2022.104191, 2022.

Yamazaki, D.: The global hydrodynamic model CaMa-Flood (version 3.6. 2)., 2014.

Yamazaki, D., Ikeshima, D., Sosa, J., Bates, P. D., Allen, G. H., and Pavelsky, T. M.: MERIT Hydro: A High-Resolution Global Hydrography Map Based on Latest Topography Dataset, Water Resour. Res., 55, 5053–5073, https://doi.org/10.1029/2019WR024873, 2019.

Zheng, K., Lin, P., and Yin, Z.: SHIFT: A DEM-Based Spatial Heterogeneity Improved Mapping of Global Geomorphic Floodplains [Dataset], https://doi.org/10.5281/zenodo.10440609, 2023.

Zomer, R. J., Xu, J., and Trabucco, A.: Version 3 of the Global Aridity Index and Potential Evapotranspiration Database, Sci. Data, 9, 409, https://doi.org/10.1038/s41597-022-01493-1, 2022.